Second-Order Nonlinear Optical Processes on a CMOS-Compatible 8-Inch Aluminum Nitride Photonics Platform

Nanxi Li[a]*, Hyo Jun Joo[a], Yangyang Zhuge[a,b], Wing Wai Chung[a], Yanmei Cao[a], Zhan Jiang Quek[a], Landobasa Y M Tobing[a,c], Chong Pei Ho[a], Dawn T. H. Tan[d], Chengkuo Lee[b], and Xianshu Luo[a,c]

[a]Institute of Microelectronics (IME), Agency for Science, Technology and Research (A*STAR), 2 Fusionopolis Way, Innovis #08-02, Singapore 138634, Republic of Singapore
[b]Center for Intelligent Sensors and MEMS, Department of Electrical and Computer Engineering, National University of Singapore, 4 Engineering Drive 3, Singapore, 117583
[c]National Semiconductor Translation and Innovation Centre (NSTIC), 1 Fusionopolis Way, #19-10 Connexis North, Singapore, 138632
[d]Photonic Devices and Systems Group, Singapore University of Technology and Design, 8 Somapah Road, Singapore, 487372

** Email address: linx1@a-star.edu.sg*

ABSTRACT

Aluminum nitride (AlN) is an emerging CMOS-compatible material for integrated photonics and can be deposited at wafer scale using a single-step physical vapor deposition process. Compared with conventional silicon photonics materials, AlN uniquely offers both a strong second-order nonlinear optical response and intrinsic piezoelectric properties, enabling efficient second-order nonlinear optical generation and on-chip tuning functionalities. In this work, we demonstrate significant second-order nonlinear optical processes in an AlN microring resonator fabricated on a CMOS-compatible 8-inch AlN photonics platform. The microring exhibits an intrinsic quality factor exceeding one million. When pumped near 1580 nm, pronounced second-harmonic generation (SHG) around 790 nm is observed using a visible-wavelength spectrum analyzer, with a side-mode suppression ratio exceeding 20 dB. The demonstrated second-order nonlinear optical performance on a wafer-scale, CMOS-compatible AlN photonics platform highlights its strong potential for integrated frequency-comb generation and applications in AR/VR, biosensing, and quantum photonics.

Keywords: Integrated optics devices; Integrated optics materials.

INTRODUCTION

Silicon integrated photonics has emerged as a cost-effective and scalable platform for optical communication, signal processing, and sensing applications, owing to its compatibility with mature complementary metal–oxide–semiconductor (CMOS) fabrication technology [1–7]. In parallel, silicon nitride (SiN) waveguides have been extensively developed to achieve ultra-low propagation loss, enabling high-Q resonators and broadband frequency comb generation [8–14]. However, conventional silicon-based photonic materials, including silicon and SiN, lack an intrinsic second-order nonlinear optical response ($\chi^{(2)}$), which fundamentally limits their efficiency in second-order nonlinear processes such as second-harmonic generation (SHG), sum-frequency generation, and electro-optic modulation.

To overcome this limitation, alternative $\chi^{(2)}$-active materials have been actively explored. Lithium niobate (LN) has demonstrated strong second-order nonlinearity and excellent electro-optic performance, leading to rapid advances in thin-film lithium niobate photonics [15–19]. Nevertheless, the heterogeneous integration of LN with CMOS-compatible platforms remains challenging due to material incompatibility, fabrication complexity, and wafer-scale scalability issues. In contrast, aluminum nitride (AlN) has emerged as a promising CMOS-compatible photonic material that intrinsically supports $\chi^{(2)}$ nonlinearity while maintaining excellent optical transparency from the ultraviolet to the infrared, low optical loss, and strong piezoelectric properties [20–24]. Importantly, AlN thin films can be deposited at wafer scale using physical vapor deposition techniques, enabling direct integration with silicon substrates in a CMOS-compatible process flow [21,25–27].

The coexistence of second-order nonlinearity and piezoelectricity in AlN enables a wide range of nonlinear and electro-optical functionalities, including SHG, optical parametric oscillation, electro-optic modulation, and frequency comb generation [28–32]. In particular, AlN microring resonators with high intrinsic quality factors have been shown to support efficient nonlinear frequency conversion and broadband microcomb generation through the interplay of $\chi^{(2)}$ and $\chi^{(3)}$ nonlinear processes [33]. Despite these advances, the realization of wafer-scale, CMOS-compatible AlN photonic platforms that simultaneously support high-Q resonators, efficient second-order nonlinear processes, and near-visible frequency conversion remains an active area of research.

In this work, we report second-order nonlinear optical processes on a CMOS-compatible 8-inch aluminum nitride photonics platform. High-Q AlN microring resonators with intrinsic quality factors exceeding one million are fabricated using a wafer-scale process. When pumped near 1580 nm, efficient SHG around 790 nm is observed, together with near-visible frequency comb lines arising from a combination of SHG and optical parametric mixing processes. The generated near-visible comb exhibits a side-mode suppression ratio exceeding 20 dB, indicating good spectral purity. These results highlight the potential of wafer-scale AlN photonics for integrated nonlinear optics, frequency comb generation, and applications spanning spectroscopy, bio-sensing, and quantum photonics.

ALUMINUM NITRIDE DEVICE PREPARATION AND MECHANISM

The SHG device follows the similar design reported in Ref. [34] and is fabricated on the same platform described in Ref. [25,27,35]. An ~730 nm-thick AlN thin film is deposited on thermally grown SiO_2 on a Si substrate using a sputtering process. We developed an in-house etching recipe that yields AlN waveguides with highly vertical sidewalls. A cross-sectional image of the etched AlN waveguide is shown in Fig. 1(a), demonstrating a sidewall angle exceeding 80°.

The wafer-scale process continues with deep-trench etching and dicing, followed by an annealing step to reduce the waveguide propagation loss. The diced 8-inch wafer is shown in Fig 1(b). A schematic of the SHG device is presented in Fig. 1(c), where an AlN microring resonator is evanescently coupled to a bus waveguide. The microring exhibits an intrinsic Q-factor exceeding 1 million (Ref. [34]), enabling efficient nonlinear optical processes.

Frequency-comb generation in the ~1600 nm range arises from the third-order nonlinear effect of four-wave mixing, whereas comb generation near 800 nm results from SHG, enabled by the intrinsic second-order nonlinearity of AlN.

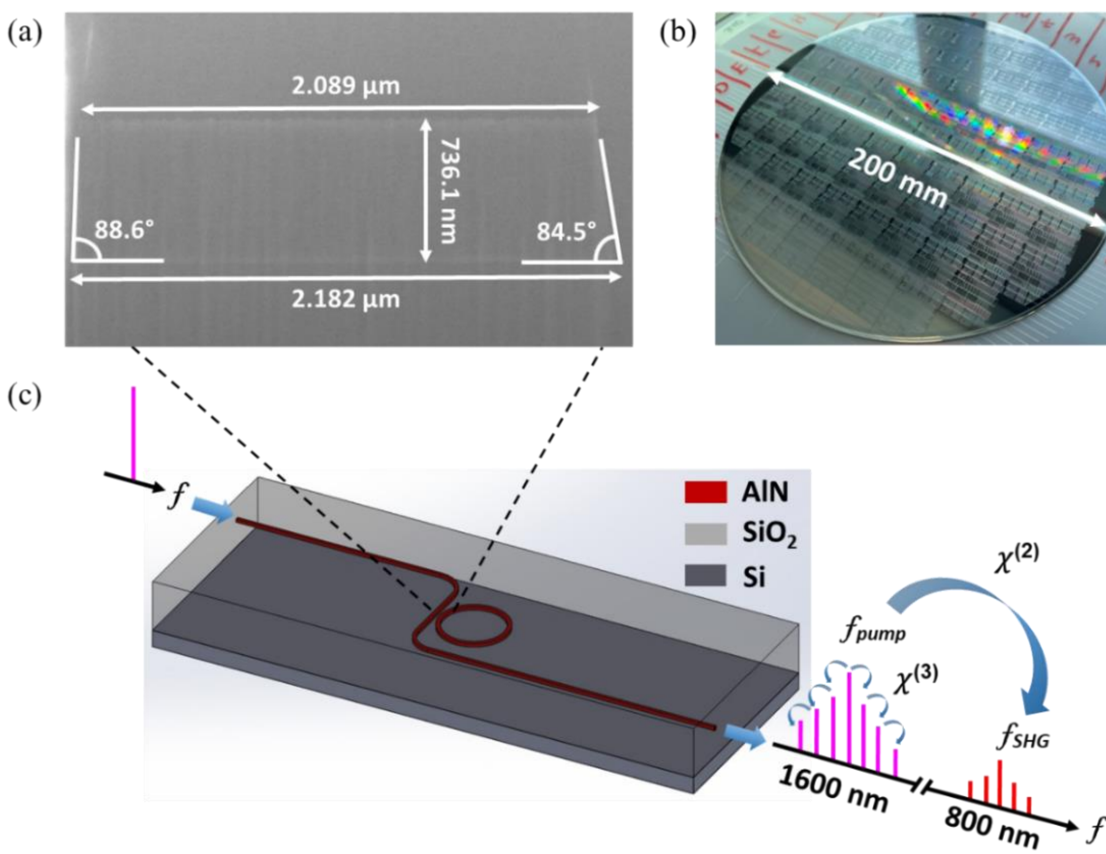

Figure 1. (a) Cross-sectional SEM image of a patterned AlN waveguide embedded in SiO_2. (b) Photograph of the fabricated 8-inch AlN wafer on a CMOS-compatible platform. (c) Schematic of the SHG device, with the nonlinear optical generation mechanisms around 1600 nm and 800 nm illustrated.

SECOND-ORDER NONLINEAR OPTICAL PROCESSES CHARACTERIZATION

The fabricated device is pumped using a tunable laser (Keysight N7776C) cascaded with an L-band high-power erbium-doped fiber amplifier (EDFA, Amonics AEDFA-L-36-R-FA), as schematically illustrated in Fig. 2(a). The pump wavelength is slowly tuned into the microring resonance with a step size of 0.01 nm, enabling optical frequency comb generation. To simultaneously characterize the generated comb lines in both the infrared (IR) and visible wavelength ranges, the output is split into two paths and analyzed by two spectrum analyzers: an IR spectrum analyzer (Yokogawa AQ6370B) and a visible spectrum analyzer (Thorlabs CCS200). The simultaneously recorded IR and visible spectra are shown in Fig. 2(b) and Fig. 2(c), respectively.

In the IR band, distinct comb states are observed as the pump wavelength is finely tuned across the microring resonance. In the visible band, only four comb lines are observed at this preliminary stage, which is mainly attributed to the limited nonlinear conversion efficiency and the limit of detection (LOD) of the visible spectrometer. Notably, the observed near-visible comb lines exhibit a side-mode suppression ratio exceeding 20 dB, indicating good spectral purity despite the limited line number.

Since the IR and near-visible spectra are acquired simultaneously, the corresponding comb lines can be directly compared. As explicitly labeled in Fig. 2(b) and Fig. 2(c), the second and fourth near-visible comb lines (counting from the shorter-wavelength side, at 791 nm and 816 nm, respectively) satisfy the second-harmonic relation,

$$\lambda_{\mathrm{nvis}} = \lambda_{\mathrm{IR}}/2,$$

corresponding to the IR comb lines at 1582 nm and 1632 nm, respectively. This one-to-one wavelength mapping confirms that these near-visible peaks originate from SHG of the corresponding IR comb lines.

By contrast, the remaining near-visible comb lines, observed at 779 nm and 803 nm (as indicated in Fig. 2(c)), do not coincide with the simple SHG mapping of any prominent IR comb lines. Instead, their wavelengths satisfy the energy-conservation (frequency-matching) condition of optical parametric mixing,

$$\omega_{\mathrm{nvis}} = \omega_{IR1} \pm \omega_{\mathrm{IR2}},$$

or equivalently,

$$1/\lambda_{\mathrm{nvis}} = 1/\lambda_{IR1} \pm 1/\lambda_{\mathrm{IR2}},$$

for example,

$$1/779\ \mathrm{nm} = 1/1536\ \mathrm{nm} + 1/1582\ \mathrm{nm},\ 1/803\ \mathrm{nm} = 1/1582\ \mathrm{nm} + 1/1632\ \mathrm{nm}.$$

This wavelength relation indicates that these near-visible lines are generated through optical parametric oscillation (OPO) rather than pure SHG. Consequently, the observed near-visible comb spectrum arises from a combination of SHG and parametric mixing processes.

It is worth noting that the number of near-visible comb lines observed at this stage remains limited. As discussed above, increasing the pump-wavelength tuning resolution across the microring resonance and further increasing the pump power are expected to enable the generation of additional near-visible comb lines [36].

In addition, when the pump laser is coupled into resonance, green fluorescence is clearly visible to the naked eye, originating from third-harmonic generation (THG). A grayscale optical image of the device under pumping conditions is shown as the inset above the "DUT" label in Fig. 2(a). Owing to the grayscale imaging mode, the green emission cannot be distinguished in the optical image, although it is directly observable by eye. While the green fluorescence is too weak to be detected by the visible spectrum analyzer, its wavelength and the corresponding IR wavelength are expected to satisfy the third-harmonic relation,

$$\lambda_{\mathrm{green}} = \lambda_{\mathrm{IR}}/3.$$

Alternative techniques reported in ref.[21] may be employed to directly capture comb lines in the green wavelength range.

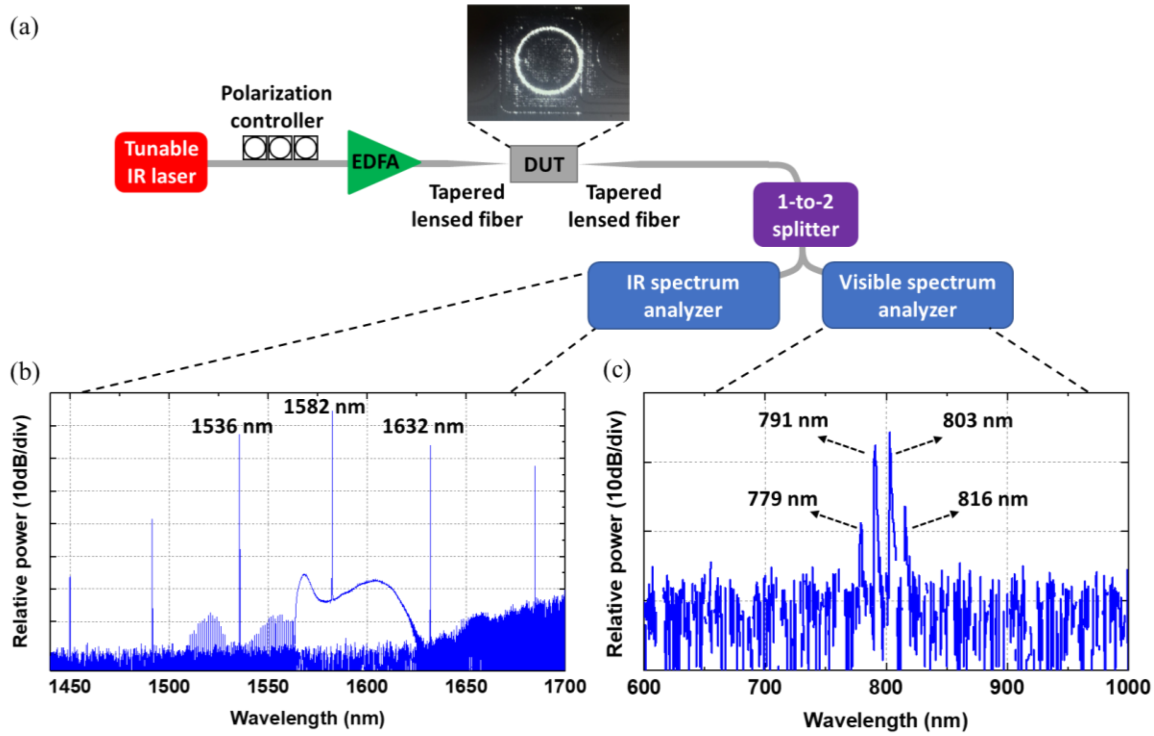

Figure 2. (a) Schematic of the experimental setup for optical frequency-comb characterization. A tunable IR laser amplified by a high-power L-band EDFA pumps the AlN microring resonator via tapered lensed fibers. The output signal is split into two paths and simultaneously analyzed by an IR spectrum analyzer and a visible spectrum analyzer. The inset shows a grayscale optical image of the device under test (DUT) during pumping; green fluorescence originating from third-harmonic generation (THG) is visible to the naked eye but cannot be distinguished in the grayscale image. (b) Simultaneously measured IR optical spectrum showing the generated frequency-comb lines as the pump wavelength is tuned into resonance. The wavelengths of representative IR comb lines are explicitly labeled. (c) Corresponding near-visible optical spectrum acquired simultaneously with (b), with the wavelengths of the observed near-visible comb lines explicitly indicated. The labeled peaks reveal near-visible comb lines generated through SHG and OPO processes.

CONCLUSION

In summary, we have demonstrated second-order nonlinear optical processes on a CMOS-compatible 8-inch aluminum nitride (AlN) photonics platform. High-Q AlN microring resonators with intrinsic quality factors exceeding one million enable efficient nonlinear interactions under near-IR pumping. When pumped around 1580 nm, pronounced second-harmonic generation near 790 nm is observed, accompanied by near-visible frequency comb lines originating from a combination of SHG and optical parametric mixing. The generated near-visible comb exhibits a side-mode suppression ratio exceeding 20 dB, indicating good spectral purity.

These results establish wafer-scale AlN photonics as a promising platform for integrated second-order nonlinear optics, offering opportunities for efficient frequency conversion, frequency comb generation, and applications in spectroscopy, bio-sensing, and quantum photonics. Future work will focus on device and dispersion optimization to further enhance nonlinear conversion efficiency and to enable systematic characterization of conversion performance.

ACKNOWLEDGEMENTS

This work is supported by Agency for Science, Technology and Research under grant no. M23M5a0069 for device fabrication, M23M6c0109 for results analysis, and National Research Foundation (NRF) under grant no. NRF-F-CRP-2024-0006 for device characterization. The authors acknowledge helpful discussions with Prof. Chee Wei Wong and Tristan Melton from UCLA on testing setup verification. We appreciate Xiaodong Shi and Di Zhu for assistance on device characterization. We used ChatGPT (OpenAI) to improve the readability and language of this manuscript; all substantive content and conclusions were developed by the authors.

REFERENCES

[1] Reed, G. T., Mashanovich, G., Gardes, F. Y. and Thomson, D. J., "Silicon optical modulators," Nature Photon **4**(8), 518–526 (2010).

[2] Magden, E. S., Li, N., Raval, M., Poulton, C. V., Ruocco, A., Singh, N., Vermeulen, D., Ippen, E. P., Kolodziejski, L. A. and Watts, M. R., "Transmissive silicon photonic dichroic filters with spectrally selective waveguides," Nat. Commun. **9**(1), 3009 (2018).

[3] Atabaki, A. H., Moazeni, S., Pavanello, F., Gevorgyan, H., Notaros, J., Alloatti, L., Wade, M. T., Sun, C., Kruger, S. A., Meng, H., Al Qubaisi, K., Wang, I., Zhang, B., Khilo, A., Baiocco, C. V., Popović, M. A., Stojanović, V. M. and Ram, R. J., "Integrating photonics with silicon nanoelectronics for the next generation of systems on a chip," Nature **556**(7701), 349–354 (2018).

[4] Purnawirman, Li, N., Magden, E. S., Singh, G., Moresco, M., Adam, T. N., Leake, G., Coolbaugh, D., Bradley, J. D. B. and Watts, M. R., "Wavelength division multiplexed light source monolithically integrated on a silicon photonics platform," Opt. Lett. **42**(9), 1772–1775 (2017).

[5] Shekhar, S., Bogaerts, W., Chrostowski, L., Bowers, J. E., Hochberg, M., Soref, R. and Shastri, B. J., "Roadmapping the next generation of silicon photonics," Nat Commun **15**(1), 751 (2024).

[6] Sorace-Agaskar, C., Callahan, P. T., Shtyrkova, K., Baldycheva, A., Moresco, M., Bradley, J., Peng, M. Y., Li, N., Magden, E. S., Purnawirman, Sander, M. Y., Leake, G., Coolbaugh, D. D., Watts, M. R. and Kärtner, F., "Integrated Mode-Locked Lasers in a CMOS-Compatible Silicon Photonic Platform," CLEO: 2015, SM2I.5, Optical Society of America, San Jose, California (2015).

[7] Singh, N., Xin, M., Li, N., Vermeulen, D., Ruocco, A., Magden, E. S., Shtyrkova, K., Ippen, E., Kärtner, F. X. and Watts, M. R., "Silicon Photonics Optical Frequency Synthesizer," Laser Photonics Rev., 1900449 (2020).

[8] Marin-Palomo, P., Kemal, J. N., Karpov, M., Kordts, A., Pfeifle, J., Pfeiffer, M. H. P., Trocha, P., Wolf, S., Brasch, V., Anderson, M. H., Rosenberger, R., Vijayan, K., Freude, W., Kippenberg, T. J. and Koos, C., "Microresonator-based solitons for massively parallel coherent optical communications," Nature **546**(7657), 274–279 (2017).

[9] Kippenberg, T. J., Gaeta, A. L., Lipson, M. and Gorodetsky, M. L., "Dissipative Kerr solitons in optical microresonators," Science **361**(6402), eaan8083 (2018).

[10] Gaeta, A. L., Lipson, M. and Kippenberg, T. J., "Photonic-chip-based frequency combs," Nat. Photon. **13**(3), 158–169 (2019).

[11] Li, N., Chen, G., Lim, L. W., Ho, C. P., Xue, J., Fu, Y. H. and Lee, L. Y. T., "Fully integrated electrically driven optical frequency comb at communication wavelength," Nanophotonics **11**(13), 2989–3006 (2022).

[12] Riemensberger, J., Lukashchuk, A., Karpov, M., Weng, W., Lucas, E., Liu, J. and Kippenberg, T. J., "Massively parallel coherent laser ranging using a soliton microcomb," Nature **581**(7807), 164–170 (2020).

[13] Chang, L., Liu, S. and Bowers, J. E., "Integrated optical frequency comb technologies," Nat. Photon. **16**(2), 95–108 (2022).

[14] Xie, Y., Li, J., Zhang, Y., Wu, Z., Zeng, S., Lin, S., Wu, Z., Zhou, W., Chen, Y. and Yu, S., "Soliton frequency comb generation in CMOS-compatible silicon nitride microresonators," Photon. Res., PRJ **10**(5), 1290–1296 (2022).

[15] Wang, C., Zhang, M., Chen, X., Bertrand, M., Shams-Ansari, A., Chandrasekhar, S., Winzer, P. and Lončar, M., "Integrated lithium niobate electro-optic modulators operating at CMOS-compatible voltages," Nature **562**(7725), 101–104 (2018).

[16] Pohl, D., Reig Escalé, M., Madi, M., Kaufmann, F., Brotzer, P., Sergeyev, A., Guldimann, B., Giaccari, P., Alberti, E., Meier, U. and Grange, R., "An integrated broadband spectrometer on thin-film lithium niobate," Nat. Photon. **14**(1), 24–29 (2020).

[17] Zhu, D., Shao, L., Yu, M., Cheng, R., Desiatov, B., Xin, C. J., Hu, Y., Holzgrafe, J., Ghosh, S., Shams-Ansari, A., Puma, E., Sinclair, N., Reimer, C., Zhang, M. and Lončar, M., "Integrated photonics on thin-film lithium niobate," Adv. Opt. Photon., **13**(2), 242–352 (2021).

[18] Chen, G., Li, N., Ng, J. D., Lin, H.-L., Zhou, Y., Fu, Y. H., Lee, L. Y. T., Yu, Y., Liu, A.-Q. and Danner, A. J., "Advances in lithium niobate photonics: development status and perspectives," Adv. Photonics **4**(3), 034003 (2022).

[19] Shams-Ansari, A., Renaud, D., Cheng, R., Shao, L., He, L., Zhu, D., Yu, M., Grant, H. R., Johansson, L., Zhang, M., Lončar, M. and Lončar, M., "Electrically pumped laser transmitter integrated on thin-film lithium niobate," Optica **9**(4), 408–411 (2022).

[20] Li, N., Ho, C. P., Zhu, S., Fu, Y. H., Zhu, Y. and Lee, L. Y. T., "Aluminium nitride integrated photonics: a review," Nanophotonics **10**(9), 2347–2387 (2021).

[21] Jung, H., Stoll, R., Guo, X., Fischer, D. and Tang, H. X., "Green, red, and IR frequency comb line generation from single IR pump in AlN microring resonator," Optica **1**(6), 396–399 (2014).
[22] Guo, X., Zou, C.-L. and Tang, H. X., "Second-harmonic generation in aluminum nitride microrings with 2500%/W conversion efficiency," Optica **3**(10), 1126–1131 (2016).
[23] Li, N., Lim, L. W., Xue, J., Ho, C. P., Zhu, S., Fu, Y. H. and Lee, L. Y. T., "Aluminum Nitride Nanophotonic Phased Array on an 8-inch Silicon Wafer," CLEO 2023, paper AM3M.5, Optica Publishing Group (2023).
[24] Liu, X., Bruch, A. W. and Tang, H. X., "Aluminum nitride photonic integrated circuits: from piezo-optomechanics to nonlinear optics," Adv. Opt. Photon., **15**(1), 236–317 (2023).
[25] Li, N., Ho, C. P., Cao, Y., Zhu, S., Chen, G. F. R., Fu, Y. H., Zhu, Y., Tan, D. T. H. and Lee, L. Y. T., "Aluminum Nitride Photonics Platforms on Silicon Substrate," CLEO 2021, paper STh2H.3, Optical Society of America (2021).
[26] Xiong, C., Pernice, W. H. P. and Tang, H. X., "Low-Loss, Silicon Integrated, Aluminum Nitride Photonic Circuits and Their Use for Electro-Optic Signal Processing," Nano Lett. **12**(7), 3562–3568 (2012).
[27] Li, N., Tobing, L. Y. M., Zhu, S. and Xue, J., "High-Q Microdisk Resonator on Aluminum Nitride Photonics Platform," CLEO 2024, paper JTh2A.28, Optica Publishing Group (2024).
[28] Jung, H., Xiong, C., Fong, K. Y., Zhang, X. and Tang, H. X., "Optical frequency comb generation from aluminum nitride microring resonator," Opt. Lett. **38**(15), 2810–2813 (2013).
[29] Jung, H., Fong, K. Y., Xiong, C. and Tang, H. X., "Electrical tuning and switching of an optical frequency comb generated in aluminum nitride microring resonators," Opt. Lett. **39**(1), 84–87 (2014).
[30] Bruch, A. W., Liu, X., Guo, X., Surya, J. B., Gong, Z., Zhang, L., Wang, J., Yan, J. and Tang, H. X., "17 000%/W second-harmonic conversion efficiency in single-crystalline aluminum nitride microresonators," Appl. Phys. Lett. **113**(13), 131102 (2018).
[31] Jung, H., Gong, Z., Liu, X., Guo, X., Zou, C. and Tang, H. X., "Stokes and anti-Stokes Raman scatterings from frequency comb lines in poly-crystalline aluminum nitride microring resonators," Opt. Express **27**(16), 22246–22253 (2019).
[32] Xiong, C., Pernice, W. H. P., Sun, X., Schuck, C., Fong, K. Y. and Tang, H. X., "Aluminum nitride as a new material for chip-scale optomechanics and nonlinear optics," New J. Phys. **14**(9), 095014 (2012).
[33] Bruch, A. W., Liu, X., Gong, Z., Surya, J. B., Li, M., Zou, C.-L. and Tang, H. X., "Pockels soliton microcomb," Nat. Photon. (2020).
[34] Li, N., Zhuge, Y., Chung, W. W., Xu, S., Cao, Y., Quek, Z. J., Tobing, L. Y. M., Ho, C. P., Tan, D. T. H., Lee, C. and Luo, X., "Broadband Frequency Comb Generation on CMOS-Compatible 8-inch Aluminum Nitride Photonics Platform," CLEO 2025, SS185_5, Optica Publishing Group, Long Beach, California (2025).
[35] Zhu, S., Zhong, Q., Li, N., Hu, T., Dong, Y., Xu, Z., Zhou, Y., Fu, Y. H. and Singh, N., "Integrated ScAlN Photonic Circuits on Silicon Substrate," CLEO 2020, STu3P.5, Optical Society of America, Washington, DC (2020).
[36] Liu, X., Sun, C., Xiong, B., Wang, L., Wang, J., Han, Y., Hao, Z., Li, H., Luo, Y., Yan, J., Wei, T., Zhang, Y. and Wang, J., "Generation of multiple near-visible comb lines in an AlN microring via $\chi(2)$ and $\chi(3)$ optical nonlinearities," Appl. Phys. Lett. **113**(17), 171106 (2018).